Impacts of organic aerosols and its oxidation level on CCN activity from measurement at a suburban site in China

Fang Zhang[1,2], Zhanqing Li*[1,2,3], Yanan Li[1,2], Yele Sun[4], Zhenzhu Wang[5], Ping Li[1,2], Li Sun[6], Pucai Wang[7], Maureen Cribb[3], Chuanfeng Zhao[1,2], Tianyi Fan[1,2], Xin Yang[1,2], Qingqing Wang[4]

[1]*State Key Laboratory of Earth Surface Processes and Resource Ecology, College of Global Change and Earth System Science, Beijing Normal University, Beijing 100875, China*
[2]*Joint Center for Global Change Studies, Beijing 100875, China*
[3]*Earth System Science Interdisciplinary Center and Department of Atmospheric and Oceanic Science, University of Maryland, College Park, Maryland, USA.*
[4]*State Key Laboratory of Atmospheric Boundary Layer Physics and Atmospheric Chemistry, Institute of Atmospheric Physics, Chinese Academy of Sciences, Beijing 100029, China*
[5]*Key Laboratory of Atmospheric Composition and Optical Radiation, Anhui Institute of Optics and Fine Mechanics, Chinese Academy of Sciences, Hefei 230031, China*
[6] *Liaoning Weather Modification Office, Shenyang, 112000, China*
[7]*Key Laboratory of Middle Atmosphere and Global Environment Observation (LAGEO), Institute of Atmospheric Physics, Chinese Academy of Sciences, 100029 Beijing, China*

***correspondence to*: Z. Li (zli@atmos.umd.edu)**

Abstract

This study is concerned with the impacts of organic aerosols on CCN activity based on field measurements made at a suburban site in north China. The sensitivity of the estimated CCN number concentration (N_{CCN}) to both volume fraction of organic material (x_{org}) and aerosol oxidation level (using f_{44}, the fraction of m/z 44 in aerosol organic material) are examined. A strong dependence of CCN number concentration (N_{CCN}) on the x_{org} and f_{44} was noted. The sensitivity of N_{CCN} to volume fraction of organics increased with increasing x_{org}. The impacts of the aerosol particles oxidization or aging level on estimating N_{CCN} were also very significant. When the particles were mostly composed of organics (x_{org}>60%), the N_{CCN} at the supersaturation of 0.075% and 0.13% was underestimated by 46% and 44% respectively if aerosol particles were freshly emitted with primary organics (f_{44}<11%); while the underestimation decreased to 32% and 23% at the corresponding supersaturations if the particles were with more hygroscopic secondary organics(f_{44}>15%). The N_{CCN} at the supersaturation of 0.76% was underestimated by 11% and 4% respectively at f_{44}<11% and f_{44}>15%. But for the particles composed of low organics (e.g. x_{org}<40%), the effect caused by the f_{44} was quite insignificant both at high and low supersaturations. This is due to that the overall hygroscopicity of the particles is dominated by inorganics such as sulfate and nitrate, which are more hygroscopic than organic compounds. Our results indicated that it would decrease the uncertainties in estimating N_{CCN} and lead to a more accurate estimation of N_{CCN} to increase the proportion of secondary organics, especially when the composition of the

aerosols is dominated by organics. The applicability of the CCN activation spectrum obtained at Xinzhou to the Xianghe site, about 400 km to the northeast of Xinzhou, was investigated, with the aim of further examining the sensitivity of N_{CCN} to aerosol type. Overall, the mean CCN efficiency spectrum derived from Xinzhou performs well at Xianghe when the supersaturation levels are > 0.2% (overestimation of 2-4%). However, N_{CCN} was overestimated by ~20% at supersaturation levels of < 0.1%. This suggests that the overestimation is mainly due to the smaller proportion of aged and oxidized organic aerosols present at Xianghe compared with Xinzhou.

1. Introduction

To reduce the uncertainty of aerosol indirect effects on the radiative balance of the atmosphere, it is important to gain a good knowledge of the ability of aerosol particles to form cloud condensation nuclei (CCN) at the typical supersaturations found in the atmosphere. The CCN activity of aerosol particles is governed by the Köhler theory (Köhler, 1936). This theory determines CCN from aerosol particle size and physicochemical properties, which include the molar volume, activity coefficient, and effect on surface tension (McFiggans et al., 2006). These properties, however, are difficult to measure.

Researchers have proposed single-parameter models to parameterize the CCN activation and hygroscopicity of multi-component aerosols (Hudson and Da, 1996; Rissler et al., 2006; Petters and Kreidenweis, 2007; Wex et al., 2007). Field experiments have been conducted with the aim of better characterizing particle physicochemical parameters influencing cloud CCN activation. Due to the large spatial variability of aerosol types and compositions, the CCN activation efficiency varies greatly over different regions. CCN number concentrations (N_{CCN}) can often be better predicted in the background atmosphere (Chuang et al., 2000; Dusek et al., 2003; VanReken et al., 2003; Snider et al., 2003; Rissler et al., 2004; Gasparini et al., 2006; Stroud et al., 2007; Bougiatioti et al., 2009).

The largest errors are associated with urban emissions (Sotiropoulou et al., 2007). This is likely due to the organics component of aerosol particles, which have the largest uncertainty and are not fully understood. Biomass burning aerosols and secondary organics formed from the oxidation of common biogenic emissions are often more difficult to activate (Mircea et al., 2005; VanReken et al., 2005; Lee et al., 2006; Varutbangkul et al., 2006; Clarke et al., 2007; Rose et al., 2010; Engelhart et al.,

2012; Paramonov et al., 2013; Lathem et al., 2013; Mei et al., 2013b; Zhang et al., 2014). Particles with aged/oxidized secondary organic components (e.g., organic acids) have been shown to be more hygroscopic (Raymond and Pandis, 2002; Hartz et al., 2006; Bougiatioti et al., 2011), but still much less hygroscopic than inorganic species. The sensitivity of estimated N_{CCN} to organics have been examined in a number of recent studies (Wang et al., 2008; Reutter et al., 2009; Ervens et al., 2010; Kammermann et al., 2010; Ward et al., 2010; Zhang et al., 2012; Mei et al., 2013a). It is widely known that the estimated N_{CCN} is sensitive to changes in organics due to the latter's complex components. The amounts and hygroscopicity parameter of organics (κ_{org}) vary substantially and lead to significant biases in estimating CCN concentrations and aerosol indirect forcing (Sotiropoulou et al., 2007; Hings et al., 2008; Liu and Wang, 2010). Therefore, field investigations regarding CCN activity and organics impacts, especially in heavily polluted regions, are pivotal to better parameterize CCN in climate models.

Northern China is a fast developing and densely populated region of China, where aerosol loading is high (Li et al., 2007, 2011), the particle composition is complex, and severe haze pollution episodes are common (Guo et al., 2014). In recent years, CCN measurements have been collected during field campaigns carried out in the region (Wiedensohler et al., 2009; Gunthe et al., 2011; Yue et al., 2011; Deng et al., 2011, 2013; Zhang et al., 2014). These studies have presented different perspectives on the influence of particle size and composition on CCN activity. For example, Deng et al. (2013) evaluated various schemes for CCN parameterization and recommended that the particle number size distribution (PSD) together with inferred mean size-resolved activation ratios can be used to estimate CCN number concentrations without considering the impact of particle composition. However,

Zhang et al. (2014) demonstrated that the 30–40% uncertainties in N_{CCN} are mainly associated with changes in particle composition. None of the above-mentioned studies have investigated the impact of organics on estimating N_{CCN} in Northern China. Zhang et al. (2012) noted a more significant influence of organics on CCN activity but without concerning the influences of particles oxidation or aging on CCN activity; in addition, the campaign average mass fraction of organics in their study was < 20%.

The aim of this paper is to examine the sensitivity of CCN activity to aerosol physicochemical properties (especially aerosols containing large amounts of organics, as well as the oxidation level), and also to see how much uncertainty is incurred by applying the CCN efficiency spectra measured at one site to another site in a heavily polluted region. The instrumentation and data used in the study are described in section 2. The method for calculating the hygroscopicity parameter (κ_{chem}) is introduced in section 3. The sensitivity of estimating N_{CCN} to x_{org} as well as oxidation level of organics is investigated in section 4, and the ability of the CCN efficiency spectrum observed at the Xinzhou site to represent CCN at the Xianghe site, are also presented and discussed at the last part of this section. Conclusions from the study are given in section 5.

2. Measurements and data

An intensive observation period field campaign similar to the Aerosol-CCN-Cloud Closure Experiment (Zhang et al., 2014), called the Atmosphere, Aerosol, Cloud, and CCN (A^2C^2) experiment, was conducted from 22 July to 26 August of 2014 at Xinzhou (38.24°N, 112.43°E; 1500 m above sea level), a city with a population of 0.51 million in Northern China. The site is located about 360 km southwest of the metropolitan Beijing area and about 10 km south of the local town center. The site is surrounded by agricultural land (e.g., corn) with little local pollution

plums from motor vehicles and industrial activities. Sitting between two mountains (Taihang Mountain to the east and Lüliang Mountain to the west), the site also experiences air masses from Xinzhou City to the north and from Taiyuan City to the south, the capital of Shanxi Province. Air masses from the northeast and southwest dominate over the site during summer. Depending on the wind direction, measurements at the Xinzhou site can detect air parcels of urban, rural, or mixed origins, including both fresh biogenic emissions around the site and aged aerosols from advection.

2.1 Instruments and measurements

During the field campaign, a Scanning Mobility Particle Sizer (SMPS), combined with a Droplet Measurement Technologies-Cloud Condensation Nuclei Counter (DMT-CCNc) (Lance et al., 2006), was used for size-resolved CCN measurements as well as particle number size distribution (PSD) measurements. The measured aerosol PSD is within the size range of 14-600 nm. Aerosol chemical composition was measured simultaneously by an Aerodyne Aerosol Chemical Speciation Monitor (ACSM) (Sun et al., 2012).

The aerosol inlet for the size distribution measurements was equipped with a TSI Environmental Sampling System (Model 3031200), which consists of a sharp-cut PM_1 cyclone and a bundled nafion dryer. The size-resolved CCN efficiency spectra were measured by coupling the DMT-CCN_C used with the SMPS (Rose et al., 2008). In this step, the particles are rapidly dried with RH < 30% upon entering the Differential Mobility Analyzer (DMA). Thus, size selection is effectively performed under dry conditions. The nafion dryer and the sheath air inside the DMA are sufficient to remove residual water associated with the ambient particles. Relative

deviations in particle diameter should be < 1%. The sample flow exiting the DMA was split into two parts: 0.3 lpm for the CPC and 0.5 lpm for the CCN counter (CCN_C). The DMA, controlled by TSI-AIM software, scanned one size distribution every five minutes. The CCN_C was operated at a total flow rate of 0.5 lpm with a sheath-to-aerosol flow ratio of 10. The inlet RH for CCNc was < 30%. During the field campaign, the mean sample temperature and pressure measured by CCN_C sensors was (24.3±1.4) ℃ and (898.4±11.7) hPa. The supersaturations levels of CCN_C were calibrated with ammonium sulfate before and after the field campaign, following the procedures outlined in Rose et al. (2008). During each CCN measurement cycle, calibrated effective supersaturations were set at 0.075%, 0.13%, 0.17%, 0.39%, and 0.75%. The overall relative error (1σ) for the supersaturation levels was estimated to be < 3.5%. The completion of a full measurement cycle took 50 minutes (10 minutes for each supersaturation level).

The measurement of non-refractory submicron aerosol species including organics, sulfate, nitrate, ammonium, and chloride were made with an ACSM. During the field campaign, ambient aerosols were drawn inside through a ½ inch (outer diameter, the inner diameter is 0.38 inch) stainless steel tube at a flow rate of ~3 L min^{-1}, of which ~84 cc min^{-1} was sub-sampled into the ACSM. An URG cyclone (Model: URG-2000-30ED) was also positioned in front of the sampling inlet to remove coarse particles with a cut-off size of 2.5 μm. Before sampling into the ACSM, aerosol particles were dried using a silica gel desiccant. The residence time in the sampling tube was ~5 s. The ACSM was operated at a time resolution of ~15 min with a scan rate of mass spectrometer at 500 ms amu^{-1} from m/z 10 to 150. Regarding the calibration of the ACSM, mono-dispersed, size-selected 300-nm ammonium nitrate particles within a range of concentrations were sampled into both the ACSM and a

condensation particle counter (CPC). The ionization efficiency (IE) was then determined by comparing the response factors of the ACSM to the mass calculated with known particle size and number concentrations from the CPC. More detailed descriptions of the operation and calibration of the ACSM are given in Sun et al. (2012) and Ng et al. (2011). The campaign averaged mass concentration of PM_1 is 31.6 μg m^{-3}.

In addition to the ACSM, the black carbon (BC) in $PM_{2.5}$ was simultaneously measured at a time resolution of 5 min by a seven-wavelength aethalometer (Model AE31, Magee Scientific Corporation). The campaign averaged mass concentration of BC is ~2.5 μg m^{-3}. During the experiment, the campaign area was generally hot and dry, with an average temperature of 21.6 ℃ and an average ambient RH of 69.5%.

2.2 Data

The raw CCN data were first filtered according to instrument recorded parameters (e.g., temperature and flow). For example, if the relative difference between the actual and preset sample flows was larger than 4%, the data are flagged as invalid. The data is also excluded if the "temperature stability" was flagged as "0". Here, the "temperature stability" refers to the T_1, T_2 and T_3 in cloud chamber of the CCNc, which is set to obtain the target supersaturations. If the average differences between preset T_1, T_2 and T_3 and the measured values are larger than 0.4 ˚C, the "temperature stability" is flagged as "0". Thus, the data is invalid and will be removed. A multiple charge correction and transfer function (Deng et al., 2011) is applied to each PSD as well as to the CCN efficiency spectrum. Size-resolved CCN and PSD data, measured with a DMT-CCNc and a SMPS (with a particle size range of 10-700 nm) on 7-21 July 2013 at Xianghe (Zhang et al., 2014), are used in this study for

157 comparisons with CCN activity at the Xinzhou site. Aerosol mass concentrations were
158 processed using the ACSM standard data analysis software (version 1.5.3.0). Detailed
159 procedures for the data analysis have been described by Ng et al. (2011) and Sun et al.
160 (2012). The size-resolved CCN activation ratio (size-resolved AR) is defined as the
161 $dN_{CCN}/dlogD_p$ divided by the $dN_{CN}/dlogD_p$. These values were measured by
162 SMPS-DMT-CCNc with particle size selection in the DMA. The bulk activation ratio
163 (bulk AR) is defined as the total CCN concentration divided by the total CN
164 concentration. The total CCN and CN number concentrations are integrated by the
165 measured CCN and CN size distribution respectively over the whole size range.

166 **3. Derivation of κ_{chem}**

167 In this study, we calculate κ_{chem} based on bulk chemical composition observations
168 made during the field campaign. The method is very similar to that used by Zhang et
169 al., (2014). As proposed by Petters and Kreidenweis (2007), κ_{chem} can be predicted
170 using a simple mixing rule based on chemical volume fractions for a given internal
171 mixture:

172 $$\kappa_{chem} = \sum_i \varepsilon_i \kappa_i \qquad (1)$$

173 where κ_i and ε_i are the hygroscopicity parameter and volume fraction, respectively, for
174 the individual (dry) components in the mixture and i is the number of components in
175 the mixture.

176 Measurements from the ACSM in Xinzhou show that the composition of
177 submicron particles was dominated by organics, followed by sulfate, ammonium, and
178 nitrate. The contribution of chloride was negligible (volume fraction of about < 2%).
179 The analysis of the anion and cation balance suggests that anionic species (NO_3^-,
180 SO_4^{2-}) were essentially neutralized by NH_4^+ over the relevant size range. For
181 refractory species, BC represented a negligible fraction of the total submicron aerosol

volume (< 3%). Sea salt and dust are usually coarse mode particles with particle sizes > 1 μm (Whitby, 1978). The contribution of such types of aerosols is thus expected to be negligible for sizes < 1 μm. Therefore, the submicron particles measured by the ACSM mainly consisted of organics, $(NH_4)_2SO_4$, and NH_4NO_3. The particle hygroscopicity is thus the volume average of the three participating species:

$$\kappa_{chem} = \kappa_{org}\varepsilon_{org} + \kappa_{(NH_4)_2SO_4}\varepsilon_{(NH_4)_2SO_4} + \kappa_{NH_4NO_3}\varepsilon_{NH_4NO_3} \quad (2)$$

Here, the values of κ for $(NH_4)_2SO_4$ and NH_4NO_3 are 0.61 and 0.67, respectively. The following linear function derived by Mei et al. (2013) was used to estimate κ_{org} in this study: $\kappa_{org} = 2.10 \times f_{44} - 0.11$, where f_{44} is the fraction of m/z 44 in total organics. The mean value of κ_{org} during the field campaign is 0.115 ±0.019.

4. Results and discussion

4.1 CCN efficiency spectra

During the field campaign at the Xinzhou site, ~790 size-resolved CCN efficiency spectra at five supersaturation levels ranging from 0.075% to 0.76% were measured. Figure 1 shows campaign averaged spectra of the measured CCN efficiency at Xinzhou for supersaturation levels of 0.075%, 0.13%, 0.17%, 0.39%, and 0.76%. The observed averaged CCN efficiency spectra during Xianghe campaign in summer 2013 are also shown. Note that the maximum activation fraction (MAF) for Xianghe site showed in Figure 1 is slight lower than that we plotted in Zhang et al.(2014). Because some data points when the MAF value >1 were not processed previously, as resulted in larger mean MAF. But in this paper, the data points with MAF > 1.0 were forced to 1 when D_p>300 nm, which could be completely activated at even lower supersaturations but the MAF would never be larger than 1.0. In Figure 1, the right panels show the mass concentration fraction of particle chemical

compositions at Xinzhou (top panel) and Xianghe (bottom panel) during their respective observation periods. Significant differences in size-resolved CCN efficiency spectra at the two sites are seen. Aerosol particles at Xinzhou activate more efficiently (higher values of AR) at a given particle diameter (D_p) for the same supersaturation level. In the other words, a larger D_p was required to reach the same activation efficiency at Xianghe. This suggests that aerosol properties at each site differ.

The slope of AR with respect to diameters near D_p when AR=50% (defined here as the cut-off diameter, D_{cut}) provides information about the heterogeneity of the composition for size-resolved particles. For an ideal case when all CCN-active particles have the same composition and size, a steep change in AR from 0 to 1 would be observed as D_p reached D_{cut}. A gradual increase in size-resolved AR with D_p suggests that aerosol particles have different hygroscopicities. The steeper slopes of AR around D_{cut} observed at Xinzhou suggest that the particle composition was less heterogeneous with more hygroscopicity than particles at the Xianghe site. This can be partially explained by the magnitudes of the mean κ_{chem} at the two sites (0.42 at Xinzhou and 0.38 at Xianghe). Also, the f_{44} is greater at Xinzhou than at Xianghe. The *m/z* 44 signal is mostly due to acids (Takegawa et al., 2007; Duplissy et al., 2011) or acid-derived species, such as esters. f_{44} is closely related to the organic oxidation level (Aiken et al., 2008). Oxidized/aged acids are generally more hygroscopic and easily activated. Moreover, the primary inorganic particles at the Xinzhou site are sulfates, with a mass fraction that is twice greater than that measured at Xianghe. Therefore, particles at the Xinzhou site consist of more hygroscopic sulfate-dominant inorganics and aged/oxidized secondary organics and can thus be more efficiently activated at a given D_p, as shown in Fig. 1.

4.2 Air mass influences on CCN activity: a case study

Because air mass back trajectories combined with ambient air measurements can be used for analyzing large-scale air pollutant transport and source identification at a receptor site (Stohl, 1996; Rousseau et al., 2004), in this study, we calculated five-day (120 hr) back trajectories using the Hybrid Single-Particle Lagrangian Integrated Trajectory (HYSPLIT) model (Draxler and Hess, 1998) with National Centers for Environmental Prediction (NCEP) reanalysis data. TrajStat software (Wang et al., 2009) has been used to calculate trajectories. The arrival height of the trajectories at the Xinzhou site was at the surface.

Three cases were selected to study air mass influences on CCN activity: (1) Case 1, 19 August 2014, 19:00-21:00 local time (LT); (2) Case 2, 9 August 2014, 03:00-10:00 LT; and (3) Case 3, 29 July 2014, 00:00-12:00 LT. Each case is associated with a different CCN efficiency spectrum, i.e., top, middle, and bottom panels of Fig. 2 are for Cases 1, 2, and 3, respectively. Their respective back trajectories are shown in Fig. 3.

In Case 1, air trajectories (red line in Fig. 3) originated from the southwest and passed through northern Shaanxi Province and northwestern Shanxi Province, then rounded back to the site from the north/northeast. So, aerosols in this case are closely associated with air parcels north/northeast of the site. The trajectories were very short, suggesting that the air flow was slow during the observational period. Under these circumstances, aerosol loading would be largely impacted by local sources around the site. A high mass fraction of organics (> 60%) with low f_{44} (~10%) and κ_{chem} (< 0.3) values was measured during the observational period. Furthermore, the PSD showed one peak mode with D_p = 56 nm and a high N_{CN} (~1.7×10^4 cm^{-3}), but low mass concentration of PM_1 (28.36 μg m^{-3}). This suggests that particles may be composed of

freshly emitted primary aerosols (the biogenic emissions from the plants and trees around the site). This type of aerosol is usually less hygroscopic with a single peak mode primarily composed of fine particles (Whitby, 1978; Hussein et al., 2005). These aerosols cannot activate efficiently. The maximum activation fraction (MAF) shown in the top right panel of Fig. 2 is less than 0.6 at all supersaturation levels for particles with D_p > 300 nm, indicating that the particles should be largely externally mixed aerosols.

In Case 2 (blue line in Fig. 3), air parcels moved rapidly from the west to the site. The site should then be influenced by the large-scale transport of air masses. For this case, aerosols contain a small amount of organics (< 30%), but have high f_{44} (~14%) and κ_{chem} values (~0.5). The PSD showed a double peak mode with an N_{CN} of ~1.3×10^4 cm^{-3} and a relatively high mass concentration of PM_1 (81.45 μg m^{-3}). The double peak mode suggests that aerosols in this case are a mixture of aerosols from local sources and from other regions (Whitby, 1978; Dal Maso et al., 2007). Because aerosols are aged and oxidized during long-distance transport, these particles are usually composed of secondary organic and inorganic components with more hygroscopicity (Weber et al., 1999; Verver et al., 2000). These aerosols can activate efficiently. The MAF is close to 1 and the slopes of AR around D_{cut} are steep at all supersaturation levels (middle right panel of Fig. 2). This CCN efficiency spectrum is similar to the ideal spectrum of pure ammonium sulfate.

In Case 3 (green line in Fig. 3), air parcels travelled from the northwest to the site. Air masses arriving at the site in this case had passed over densely populated regions with more heavy pollution. A gradual increase in size-resolved AR with D_p is seen (bottom right panel of Fig. 2). This is attributed to the diversity in aerosol hygroscopicity because of the complex nature of the chemical composition of aerosol

particles.

4.3 Correlation of N_{CN} and N_{CCN}

Figure 4 shows N_{CN} as a function of N_{CCN} for different supersaturation levels at the Xinzhou and Xianghe sites. They showed high or moderate correlations at high supersaturation levels (e.g., R^2 = 0.57 at Xinzhou and R^2 = 0.85 at Xianghe at a supersaturation level of ~0.8%), but quite poor correlations at low supersaturation levels. Although Andreae (2009) proposed using the relationship of CCN and CN, or even aerosol optical depth (AOD), to parameterize CCN in models, it would lead to large uncertainties especially when the supersaturations are low. It was noticed that there was an apparent higher degree of correlation at Xianghe site for each supersaturation than that derived at Xinzhou site. In view of the similar regimes from which the data are taken and the same instruments by which they have been collected, the discrepancy between Xianghe and Xinzhou should be caused largely by the spatial variations of aerosols types. These variations are primarily attributed to variations in aerosol particle size, i.e., the shape of the PSD as well as particle composition. As presented by Zhang et al. (2014), the relationship between bulk activation ratios and N_{CN} was complex under polluted conditions and was heavily dependent on the physicochemical properties of atmospheric aerosols.

4.4 Impact of x_{org} on N_{CCN}

Precise quantification of N_{CCN} is crucial for understanding aerosol indirect effects and characterizing these effects in models. A CCN closure study is useful to examine the controlling physical and chemical factors and to help verify experimental results. N_{CCN} is usually derived from measured aerosol properties, such as PSD and composition or hygroscopicity based on the Köhler theory. Achieving such closure

under heavily polluted conditions is more challenging, especially due to the complex effects of organics on CCN activity. In this section, we examine the sensitivity of N_{CCN} to both volume fraction of organics (x_{org}) and oxidation or aging of organics based on measurement at Xinzhou site. During the observed period, aerosols at the Xinzhou site were dominated by organics, with 12%, 23%, 39%, and 25% of the data points corresponding to x_{org} >60 %, 50%<x_{org} <60 %, 40%<x_{org} <50 % and x_{org} <40 %, respectively. For the purpose of examining the sensitivity of estimated N_{CCN} to x_{org} and oxidation/aging level, we sorted the size-resolved CCN data when the x_{org} >60 %, 50%<x_{org} <60 %, 40%<x_{org} <50 % and x_{org} <40 %. Furthermore, for each level of x_{org}, we tested the impacts on N_{CCN} estimation both from the most oxidized (with f_{44} of higher than 15%) and least oxidized (those primary organic aerosols with f_{44} of lower than 11%) organic particles. For example, the size-resolved CCN data points during the period when x_{org} >60 % and also f_{44} >15% was averaged to generate the averaged CCN efficiency spectra at the five supersaturations respectively. Then we used the produced averaged CCN efficiency spectra to estimate N_{CCN}.

Estimated CCN size distributions at the five supersaturations were firstly calculated by multiplying the averaged CCN efficiency spectrum (by using the averaged CCN efficiency spectra, the aerosol particles were assumed with uniform chemical composition without considering the effects of the temporal variations of the activation curves on CCN activity) with the actually measured PSD. Then, we integrated the estimated CCN size distribution over the whole size range to generate estimated N_{CCN}. While the measured CCN size distributions are integrated to produce the observed N_{CCN}.

Observed and estimated N_{CCN} at four supersaturation levels (0.075%, 0.13, 0.17 and 0.76%) were showed in Fig 5. The data points presented more disperse and

weaker correlations at lower supersaturations. The sensitivity of N_{CCN} to volume fraction of organics increased with increasing x_{org}. This is especially for the case of these primary organic particles with f_{44}<11%: the slopes obtained from a linear fit of estimated and measured N_{CCN} in Fig 6 decreased rapidly (almost with a decrease of ~50%) when the x_{org} varied from <40% to >60% at supersaturations of 0.075%, while it didn't exhibit a lot of reduction (merely ~10%) along with the increasing of x_{org} at the supersaturation of 0.76%. N_{CCN} was estimated most accurately at higher supersaturation levels. This is likely because a large fraction of particles was already CCN-active. Also, particle composition has relatively less influence on CCN activation at high supersaturations (Twohy and Anderson, 2008). For the oxidized or aged particles with f_{44}>15%, the slopes still follow the similar tendency with the variations of x_{org} at low and high supersaturations but changed more smoothly to the x_{org} attributing to the oxidized/aged organic particles being more hygroscopic.

However, the impacts of the aerosol particles oxidization level on estimating N_{CCN} were also very significant. For example, when the particles were composed by large amounts of organics (x_{org}>60%), the N_{CCN} at the supersaturation of 0.075% and 0.13% was underestimated by 46% and 44% respectively at f_{44}<11%, while the underestimation decreased to 32% and 23% at the corresponding supersaturation level when f_{44}>15%. The N_{CCN} at ss=0.76 was underestimated by 11% and 4% respectively at f_{44}<11% and f_{44}>15%. The results showed that the estimation of N_{CCN} would be largely improved if the aerosol particles were aged with high oxidation level, especially when the chemical composition of the particles is dominated by organics. But for the particles with relative low organics (x_{org}<40%), the effect caused by the f_{44} was quite insignificant both for high and low supersaturations. In Fig 6, the slopes were all around 1.0 at the two cases of f_{44}<11% and f_{44}>15%. This can be easily

explained. When x_{org} is less than 40%, the overall hygroscopicity of the particles is dominated by inorganic species such as sulfate and nitrate, which are more hygroscopic (κ_{inorg} usually larger than 0.6) than organic compounds (κ_{org} usually smaller than 0.2). As a result, a larger fraction of particles can be activated. According to the simple mixing rule based on chemical volume fractions proposed by Petters and Kreidenweis (2007), the contribution from organics is quite small. If x_{org} is greater than 60%, organics will dominate the overall particle hygroscopicity. Particles with a large f_{44} are much more hygroscopic and thus more CCN-active. Our results indicated that increasing the proportion of secondary organics would decrease the uncertainties in estimating N_{CCN} and lead to a more accurate estimation of N_{CCN}.

4.5 Applicability of CCN efficiency spectra

As a means of testing the applicability of the CCN activation spectra, campaign mean CCN efficiency spectra at different supersaturations observed at the Xinzhou site is used to estimate N_{CCN} at the Xinzhou and Xianghe sites respectively, which helps to further examine the sensitivity of N_{CCN} to aerosol type. Data from the two sites were measured during the warm season so that the effect of temporal variations in aerosols on CCN levels is reduced. Fitted campaign mean CCN efficiency spectrum at the five supersaturations at Xinzhou (corresponding to spectra in Fig. 1) is multiplied by dry PSDs actually measured at Xinzhou and at the Xianghe site respectively. This generates estimated CCN size distributions at the two sites. They are then integrated over the whole size range (14-600 nm and 10-700 nm at the Xinzhou and Xianghe sites, respectively) to obtain the estimated N_{CCN}. The measured CCN size distributions at each site are integrated to produce the observed N_{CCN}.

Figure 7 shows estimated N_{CCN} as a function of measured N_{CCN} for different

supersaturation levels at the two sites. N_{CCN} at Xinzhou was underestimated by 4-5% at supersaturation levels of 0.39% and 0.76%, and was slightly overestimated (~2%) at Xianghe for the same supersaturation levels. Good agreement is seen at the 0.39% and 0.76% supersaturation levels for data from both sites (R^2 > 0.92). N_{CCN} at Xinzhou was underestimated by ~7% at supersaturation levels < 0.1% (R^2 = 0.87). At Xianghe, however, N_{CCN} was overestimated by 19-23% at supersaturation levels < 0.1% although the correlation between calculated and measured N_{CCN} was good. Because size-resolved CCN efficiency spectra were applied here, excluding the impact of particle size, the influence of chemical composition on CCN activation can be investigated. The poor estimates of CCN at low supersaturation levels could be attributed to the high sensitivity of N_{CCN} to chemical composition. Because the mass fractions of inorganics and organics measured at the two sites are similar (Fig. 1) and the hygroscopicity for inorganic components is fixed, this overestimation is attributed to the smaller proportion of aged and oxidized organic aerosols at Xianghe compared with aerosols at Xinzhou (f_{44} = 17% and 11% at Xinzhou and Xianghe, respectively).

5. Summary and conclusions

In this study, we have investigated the impacts of particle physicochemical properties on CCN activity based on field measurements obtained from 22 July to 26 August of 2014 in the suburb of Xinzhou, China. Five-day back trajectories combined with measurements were analyzed to examine air mass influences on CCN activity. CCN efficiency was largely reduced by local air masses, and the MAF was low to <60%, suggesting externally-mixed and the heterogeneity of particle composition for local emitted aerosols. The CCN activation efficiency was enhanced significantly when the site was under the influence of air transported from far away, during which aerosols could be mixed well with more hygroscopic secondary organic and inorganic

components. The relationship between N_{CN} and N_{CCN} was generally poor. Large errors would arise if using the former to estimate the latter, especially under low supersaturation conditions.

The sensitivity of N_{CCN} estimation to both x_{org} and f_{44} has also been examined. A strong dependence of N_{CCN} on the both two parameters was noted. The sensitivity of N_{CCN} to volume fraction and particles oxidization or aging level of organics increased with increase of x_{org}. And also this dependence weakens as the supersaturation level increases. When the particles were mostly composed of organics (x_{org}>60%), the N_{CCN} at the supersaturation of 0.075% and 0.13% was underestimated by 46% and 44% respectively if aerosol particles were freshly emitted with primary organics (f_{44}<11%); while the underestimation decreased to 32% and 23% at the corresponding supersaturations if the particles were with more hygroscopic secondary organics(f_{44}>15%). The N_{CCN} at the supersaturation of 0.76% was underestimated by 11% and 4% respectively at f_{44}<11% and f_{44}>15%. But for the particles composed of low organics (e.g. x_{org}<40%), the effect caused by the f_{44} was quite insignificant both at high and low supersaturations. This is due to that the overall hygroscopicity of the particles is dominated by inorganics such as sulfate and nitrate, which are more hygroscopic than organic compounds. Our results indicated that it would lead to a more accurate estimation of N_{CCN} to increase the proportion of secondary organics, especially when the composition of the aerosols is dominated by organics.

The applicability of the CCN efficiency spectrum measured at the Xinzhou site to the Xianghe site was examined and a good agreement was found when the supersaturation level was > 0.2%. However, N_{CCN} at the Xianghe site was overestimated by 19-23% when the supersaturation level was < 0.1%. Because of the similar mass fractions of inorganics and organics measured at the two sites, we

conclude that this overestimation was mainly caused by the smaller proportion of aged and oxidized organic aerosols at Xianghe compared with aerosols at Xinzhou.

Acknowledgements

This work was funded by the National Basic Research Program of China '973' (Grant No. 2013CB955801, 2013CB955804) and the NSCF-TAMU Collaborative Research Grant Program (Grant No. 4141101031). We also acknowledge the members of the A^2C^2 team for their hard work during the campaign, including Mr. Du Wei (from the State Key Laboratory of Atmospheric Boundary Layer Physics and Atmospheric Chemistry of the Institute of Atmospheric Physics/Chinese Academy of Sciences for carrying out the chemical composition measurements) and Mr. Yuan Cheng (from Nanjing University who helped make the size-resolved CCNc measurements).

References

Aiken, A. C., DeCarlo, P. F., Kroll, J. H., Worsnop, D. R., Huffman, J. A., Docherty, K. S., Ulbrich, I. M., Mohr, C., Kimmel, J. R., Sueper, D., Sun, Y., Zhang, Q., Trimborn, A., Northway, M., Ziemann, P. J., Canagaratna, M. R., Onasch, T. B., Alfarra, M. R., Prevot, A. S. H., Dommen, J., Duplissy, J., Metzger, A., Baltensperger, U., and Jimenez, J. L.: O/C and OM/OC ratios of primary, secondary, and ambient organic aerosols with high-resolution time-of-flight aerosol mass spectrometry, Environ. Sci. Technol., 42, 4478–4485, 2008.

Andreae, M.O.: Correlation between cloud condensation nuclei concentration and aerosol optical thickness in remote and polluted regions, Atmos. Chem. Phys., 9, 543-556, 2009.

Bougiatioti, A., Fountoukis, C., Kalivitis, N., Pandis, S. N., Nenes, A., and Mihalopoulos, N.: Cloud condensation nuclei measurements in the marine

boundary layer of the eastern Mediterranean: CCN closure and droplet growth kinetics. Atmos. Chem. Phys., 9, 7053–7066, 2009.

Bougiatioti, A., Nenes, A., Fountoukis, C., Kalivitis, N., Pandis, S. N., and Mihalopoulos, N.: Size-resolved CCN distributions and activation kinetics of aged continental and marine aerosol, Atmos. Chem. Phys., 11, 8791-8808, doi:10.5194/acp-11-8791-2011, 2011.

Chuang, P. Y., Collins, D. R., Pawlowska, H., Snider, J. R., Jonsson, H. H., Brenguier, J. L., Flagan, R. C., and Seinfeld, J. H.: CCN measurements during ACE-2 and their relationship to cloud microphysical properties, Tellus B, 52, 843–867, 2000.

Clarke, A., McNaughton, C., Kasputin, V. N., Shinozuka, Y., Howell, S., Dibb, J., Zhou, J., Anderson, B., Brekhovskikh, V., Turner, H., and Pinkerton, M.: Biomass burning and pollution aerosol over North America: Organic components and their influence on spectral optical properties and humidification response, J. Geophys. Res., 112, D12S18, doi:10.1029/2006JD007777, 2007.

Dal Maso, M., L. Sogacheva, P. P. Aalto, I. Riipinen, M. Komppula, P. Tunved, L. Korhonen, V.SUUR©\USKI, A. Hirsikko, and T. KurtEN,Aerosol size distribution measurements at four Nordic field stations: identification, analysis and trajectory analysis of new particle formation bursts, Tellus B,2007,59(3), 350-361.

Deng, Z., Zhao, C., Ma, N., Liu, F., Ran, L., Xu, W., Liang, Z., Liang, S., Huang, M., Ma, X., Zhang, Q., Quan, J., and Yan, P.: Size- resolved and bulk activation properties of aerosols in the North China Plain. Atmos. Chem. Phys., 11, 3835-3846, 2011.

Deng, Z., Zhao, C., Ma, N., Ran, L., Zhou, G., Lu, D., and Zhou, X.: An examination of parameterizations for the CCN number concentration based on in situ

478 measurements of aerosol activation properties in the North China Plain, Atmos.
479 Chem. Phys., 13, 6227–6237, doi:10.5194/acp-13-6227-2013, 2013.
480 Draxler, R., R. and Hess, G., D. 1998. An overview of the HYSPLIT 4 modeling
481 system for trajectories, dispersion, and deposition, *Aust. Meteorol. Mag.* 47, 295–
482 308.
483 Duplissy, J., DeCarlo, P. F., Dommen, J., Alfarra, M. R., Metzger, A., Barmpadimos,
484 I., Prevot, A. S. H.,Weingartner, E., Tritscher, T., Gysel, M., Aiken, A. C., Jimenez,
485 J. L., Canagaratna, M. R., Worsnop, D. R., Collins, D. R., Tomlinson, J., and
486 Baltensperger, U.: Relating hygroscopicity and composition of organic aerosol
487 particulate matter, Atmos. Chem. Phys., 11, 1155–1165,
488 doi:10.5194/acp-11-1155-2011, 2011.
489 Dusek, U., Covert, D. S., Wiedensohler, A., Neususs, C., Weise, D., and Cantrell, W.:
490 Cloud condensation nuclei spectra derived from size distributions and hygroscopic
491 properties of the aerosol in coastal south-west Portugal during ACE-2, Tellus B, 55,
492 35–53, 2003.
493 Engelhart, G. J., Hennigan, C. J., Miracolo, M. A., Robinson, A. L., and Pandis, S. N.:
494 Cloud condensation nuclei activity of fresh primary and aged biomass burning
495 aerosol, Atmos. Chem. Phys., 12, 7285–7293, doi:10.5194/acp-12-7285-2012,
496 2012.
497 Ervens, B., Cubison, M. J., Andrews, E., Feingold, G., Ogren, J.A., Jimenez, J. L.,
498 Quinn, P. K., Bates, T. S., Wang, J., Zhang, Q., Coe, H., Flynn, M., and Allan, J. D.:
499 CCN predictions using simplified assumptions of organic aerosol composition and
500 mixing state: a synthesis from six different locations, Atmos. Chem.Phys., 10,
501 4795–4807, doi:10.5194/acp-10-4795-2010, 2010.
502 Gasparini, R., Collins, D. R., Andrews, E., Sheridan, P. J., Ogren, J. A., and Hudson, J.

503 G.: Coupling aerosol size distributions and size-resolved hygroscopicity to predict
504 humidity-dependent optical properties and cloud condensation nuclei spectra., J.
505 Geophys. Res., 111, D05S13, doi:10.1029/2005JD006092, 2006.
506 Gunthe SS; Rose D; Su H; Garland RM; Achtert P; Nowak A; Wiedensohler A;
507 Kuwata M; Takegawa N; Kondo Y; Hu M; Shao M; Zhu T; Andreae MO; Pöschl
508 U (2011) Cloud condensation nuclei (CCN) from fresh and aged air pollution in
509 the megacity region of Beijing, Atmospheric Chemistry and Physics, 11,
510 pp.11023-11039. doi: 10.5194/acp-11-11023-2011
511 Guo, S., Hu, M., Zamora, M. L., Peng, J., Shang, D., Zheng, J., Zhuofei Du, Zhijun
512 Wu, Min Shao, Limin Zeng, Mario J. Molina,1, and Zhang, R. (2014).
513 Elucidating severe urban haze formation in China. Proceedings of the National
514 Academy of Sciences of the United States of America, 111(49), 17373–17378.
515 doi:10.1073/pnas.1419604111
516 Hartz, K. E. H., Tischuk, J. E., Chan, M. N., Chan, C. K., Donahue, N. M., and Pandis,
517 S. N.: Cloud condensation nuclei activation of limited solubility organic aerosol,
518 Atmos. Environ., 40, 605–617, 2006.
519 Hings, S. S., Wrobel, W. C., Cross, E. S., Worsnop, D. R., Davidovits, P., and Onasch,
520 T. B.: CCN activation experiments with adipic acid: effect of particle phase and
521 adipic acid coatings on soluble and insoluble particles, Atmos. Chem. Phys., 8,
522 3735–3748, doi:10.5194/acp-8-3735-2008, 2008.
523 Hudson, J. G. and Da, X. Y.: Volatility and size of cloud condensation nuclei, J.
524 Geophys. Res., 101, 4435–4442, 1996.
525 Hussein, T., M. Dal Maso, T. PETÄJÄ, I. K. KOPONEN, P. PAATERO, P. P.
526 AALTO, K. HÄMERI, and M. KULMALA,Evaluation of an automatic
527 algorithm for fitting the particle number size distributions, BOREAL

528 ENVIRONMENT RESEARCH, 2005,10(5), 337-355.
529 Junge, C. and McLaren, E.: Relationship of cloud nuclei spectra to aerosol size
530 distribution and composition, J. Atmos. Sci., 28, 382–390, 1971.
531 Kammermann, L., Gysel, M., Weingartner, E., Herich, H., Cziczo, D. J., Holst, T.,
532 Svenningsson, B., Arneth, A., and Baltensperger, U.: Subarctic atmospheric aerosol
533 composition: 3. Measured and modeled properties of cloud condensation nuclei, J.
534 Geophys. Res., 115, D04202, doi:10.1029/2009JD012447, 2010.
535 Köhler, H.: The nucleus in and growth of hygroscopic droplets, Trans. Faraday Soc.,
536 32, 1152–1161, doi:10.1039/TF9363201152, 1936.
537 Lance, S., Medina, J., Smith, J., and Nenes, A.: Mapping the operation of the DMT
538 continuous flow CCN counter, Aerosol Sci. Technol., 40 , 242–254, 2006.
539 Lathem, T. L., Beyersdorf, A. J., Thornhill, K. L., Winstead, E. L., Cubison, M. J.,
540 Hecobian, A., Jimenez, J. L., Weber, R. J., Anderson, B. E., and Nenes, A.: Analysis
541 of CCN activity of Arctic aerosol and Canadian biomass burning during summer
542 2008, Atmos. Chem. Phys., 13, 2735-2756, doi:10.5194/acp-13-2735-2013, 2013.
543 Lee, Y. S., Collins, D. R., Li, R. J., Bowman, K. P., and Feingold, G.: Expected
544 impact of an aged biomass burning aerosol on cloud condensation nuclei and cloud
545 droplet concentrations, J. Geophys. Res., 111, D22204, doi:10.1029/2005JD006464,
546 2006.
547 Li, Z., Chen, H., Cribb, M., Dickerson, R. E., Holben, B., Li, C., Lu, D., Luo, Y.,
548 Maring, H., Shi, G., Tsay, S.-C., Wang, P., Wang, Y., Xia, X., Zheng, Y., Yuan, T.,
549 and Zhao, F.: Preface to special section on East Asian Studies of Tropospheric
550 Aerosols: An International Regional Experiment (EASTAIRE), J. Geophys. Res.,
551 112, D22S00, doi:10.1029/2007JD008853, 2007.
552 Li, Z., Li, C., Chen, H., Tsay, S.-C., Holben, B., Huang, J., Li, B., Maring, H., Qian,

553 Y., Shi, G., Xia, X., Yin, Y., Zheng, Y., and Zhuang, G.: East Asian Studies of
554 Tropospheric Aerosols and Impact on Regional Climate (EAST‐AIRC): An
555 overview, J. Geophys. Res., 116, D00K34, doi:10.1029/2010JD015257, 2011.
556 Liu, X. and Wang, J.: How important is organic aerosol hygroscopicity to aerosol
557 indirect forcing? Environ. Res. Lett., 5, 044010,
558 doi:10.1088/1748-9326/5/4/044010, 2010.
559 McFiggans, G., Artaxo, P., Baltensperger, U., Coe, H., Facchini, M. C., Feingold, G.,
560 Fuzzi, S., Gysel, M., Laaksonen, A., Lohmann, U., Mentel, T. F., Murphy, D. M.,
561 O'Dowd, C. D., Snider, J. R., and Weingartner, E.: The effect of physical and
562 chemical aerosol properties on warm cloud droplet activation, Atmos. Chem. Phys.,
563 6, 2593–2649, doi:10.5194/acp-6-2593-2006, 2006.
564 Mei, F., Hayes, P. L., Ortega, A. M., Taylor, J. W., Allan, J. D., Gilman, J. B., Kuster,
565 W. C., de Gouw, J. A., Jimenez, J. L., and Wang, J.: Droplet activation properties
566 of organic aerosols observed at an urban site during CalNex-LA, J. Geophys. Res.,
567 118(7), 2903-2917, doi: 10.1002/jgrd.50285, 2013b.
568 Mei, F., Setyan, A., Zhang, Q., and Wang, J.: CCN activity of organic aerosols
569 observed downwind of urban emissions during CARES, Atmos. Chem. Phys., 13,
570 12155–12169,doi:10.5194/acp-13-12155-2013, 2013a.
571 Mircea, M., Facchini, M. C., Decesari, S., Cavalli, F., Emblico, L., Fuzzi, S., Vestin,
572 A., Rissler, J., Swietlicki, E., Frank, G., Andreae, M. O., Maenhaut, W., Rudich, Y.,
573 and Artaxo, P.: Importance of the organic aerosol fraction for modeling aerosol
574 hygroscopic growth and activation: a case study in the Amazon Basin, Atmos.
575 Chem. Phys., 5, 3111–3126, 2005, http://www.atmos-chem-phys.net/5/3111/2005/.
576 Ng, N. L., Herndon, S. C., Trimborn, A., Canagaratna, M. R., Croteau, P. L., Onasch,
577 T. B., Sueper, D.,Worsnop, D. R., Zhang, Q., Sun, Y. L., and Jayne, J. T.: An

578 Aerosol Chemical Speciation Monitor (ACSM) for Routine Monitoring of the
579 Composition and Mass Concentrations of Ambient Aerosol, Aerosol Sci. Tech., 45,
580 770–784, 2011.
581 Paramonov, M., Aalto, P. P., Asmi, A., Prisle, N., Kerminen, V.-M., Kulmala, M., and
582 Petäjä, T.: The analysis of size-segregated cloud condensation nuclei counter
583 (CCNC) data and its implications for aerosol-cloud interactions, Atmos. Chem.
584 Phys. Discuss., 13, 9681-9731, doi:10.5194/acpd-13-9681-2013, 2013.
585 Petters, M. D., and Kreidenweis, S. M.: A single parameter representation of
586 hygroscopic growth and cloud condensation nucleus activity, Atmos. Chem. Phys.,
587 7, 1961–1971, doi:10.5194/acp-7-1961-2007, 2007.
588 Petters, M. D. and Kreidenweis, S. M.: A single parameter representation of
589 hygroscopic growth and cloud condensation nucleus activity – Part 2: Including
590 solubility, Atmos. Chem. Phys., 8, 6273–6279, doi:10.5194/acp-8-6273-2008,
591 2008.
592 Raymond, T. M., and Pandis, S. N.: Cloud activation of single component organic
593 aerosol particles, J. Geophys. Res., 107, 4787, doi:10.1029/2002JD002159, 2002.
594 Reutter, P., Su, H., Trentmann, J., Simmel, M., Rose, D., Gunthe, S. S., Wernli, H.,
595 Andreae, M. O., and Pöschl, U.: Aerosol- and updraft-limited regimes of cloud
596 droplet formation: influence of particle number, size and hygroscopicity on the
597 activation of cloud condensation nuclei (CCN), Atmos. Chem. Phys., 9, 7067–7080,
598 doi:10.5194/acp-9-7067-2009, 2009.
599 Rissler, J., Swietlicki, E., Zhou, J., Roberts, G., Andreae, M. O., Gatti, L. V., and
600 Artaxo, P.: Physical properties of the submicrometer aerosol over the Amazon rain
601 forest during the wet to dry season transition – comparison of modeled and
602 measured CCN concentrations, Atmos. Chem. Phys., 4, 2119–2143,

603 http://www.atmos-chem-phys.net/4/2119/2004/, 2004.
604 Rissler, J., Vestin, A., Swietlicki, E., Fisch, G., Zhou, J., Artaxo, P., and Andreae, M.
605 O.: Size distribution and hygroscopic properties of aerosol particles from
606 dry-season biomass burning in Amazonia, Atmos. Chem. Phys., 6, 471–491,
607 doi:10.5194/acp-6-471-2006, 2006.
608 Rose, D., Gunthe, S. S., Mikhailov, E., Frank, G. P., Dusek, U., Andreae, M. O., and
609 Poschl, U.: Calibration and measurement uncertainties of a continuous-flow cloud
610 condensation nuclei counter (DMT-CCNC): CCN activation of ammonium sulfate
611 and sodium chloride aerosol particles in theory and experiment, Atmos. Chem.
612 Phys., 8, 1153–1179, 2008, http://www.atmos-chem-phys.net/8/1153/2008/.
613 Rose, D., Nowak, A., Achtert, P.,Wiedensohler, A., Hu, M., Shao, M., Zhang, Y.,
614 Andreae, M. O., and P ¨oschl, U.: Cloud condensation nuclei in polluted air and
615 biomass burning smoke near the mega-city Guangzhou, China – Part 1:
616 Size-resolved measurements and implications for the modeling of aerosol particle
617 hygroscopicity and CCN activity, Atmos. Chem. Phys., 10, 3365–3383,
618 doi:10.5194/acp-10-3365-2010, 2010.
619 Rousseau, D., D., Duzer, D., Etienne, J., L., Cambon, G., Jolly, D. And coauthors.
620 2004. Pollen record of rapidly changing air trajectories to the North Pole, *J.*
621 *Geophys. Res.* 109, D06116, doi:10.1029/2003JD003985.
622 Snider, J.R., Guibert, S., Brenguierand, J. L. and Putaud, J. P.: Aerosol activation in
623 marine stratocumulus clouds: Part – II K öhler and parcel theory closure studies, J.
624 Geophy. Res., 108, doi:10.1029/2002JD002692, 2003
625 Sotiropoulou, R. E. P., Nenes, A., Adams, P. J., and Seinfeld, J. H.: Cloud
626 condensation nuclei prediction error from application of K ¨ohler theory:
627 Importance for the aerosol indirect effect, J. Geophys. Res., 112, D12202,

628 doi:10.1029/2006JD007834, 2007.
629 Stohl, A. 1996, Trajectory statistics - a new method to establish source-receptor
630 relationships of air pollutants and its application to the transport of particulate
631 sulfate in Europe, *Atmos. Environ.* 30, 579–587.
632 Stroud, C. A., Nenes, A., Jimenez, J. L., DeCarlo, P., Huffman, J. A., Bruintjes, R.,
633 Nemitz, E., Delia, A. E., Toohey, D. W., Guenther, A. B., and Nandi, S.: Cloud
634 Activating Properties of Aerosol Observed during CELTIC, J. Atmos. Sci., 64, 441–
635 459, 2007.
636 Sun, Y., Wang, Z., Dong, H., Yang, T., Li, J., Pan, X., Chen, P., and Jayne, J. T.:
637 Characterization of summer organic and inorganic aerosols in Beijing, China with
638 an Aerosol Chemical Speciation Monitor, Atmos. Environ., 51, 250–259,
639 doi:10.1016/j.atmosenv.2012.01.013, 2012.
640 Takegawa, N., Miyakawa, T., Kawamura, K., and Kondo, Y.: Contribution of selected
641 di-carboxylic and omega-oxocarboxylic acids in ambient aerosol to the m/z 44
642 signal of an aerodyne aerosol mass spectrometer, Aerosol Sci. Technol., 41, 418–
643 437, doi:10.1080/02786820701203215, 2007.
644 Twohy, C. H. and Anderson, J. R.: Droplet nuclei in non-precipitating clouds:
645 composition and size matter, Environ. Res. Lett., 3, 045002,
646 doi:10.1088/1748-9326/3/4/045002, 2008.
647 VanReken, T. M., Rissman, T. A., Roberts, G. C., Varutbangkul, V., Jonsson, H. H.,
648 Flagan, R. C., and Seinfeld, J. H.: Toward aerosol/cloud condensation nuclei (CCN)
649 closure during CRYSTAL-FACE, J. Geophys. Res., 108, 4633,
650 doi:10.1029/2003JD003582, 2003.
651 VanReken, T. M., Ng, N. L., Flagan, R. C., and Seinfeld, J. H.: Cloud condensation
652 nucleus activation properties of biogenic secondary organic aerosol, J. Geophys.

Res., 110, D07206, doi:10.1029/2004JD005465, 2005.

Varutbangkul, V., Brechtel, F. J., Bahreini, R., Ng, N. L., Keywood, M. D., Kroll, J. H., Flagan, R. C., Seinfeld, J. H., Lee, A., and Goldstein, A. H.: Hygroscopicity of secondary organic aerosols formed by oxidation of cycloalkenes, monoterpenes, sesquiterpenes, and related compounds, Atmos. Chem. Phys., 6, 2367–2388, 2006.

Verver, G., F. Raes, D. Vogelezang, and D. Johnson,The 2nd Aerosol characterization Experiment (ACE-2): meteorological and chemical context, Tellus B, 2000,52(2), 126-140.

Wang, J., Lee, Y.-N., Daum, P. H., Jayne, J., and Alexander, M. L.: Effects of aerosol organics on cloud condensation nucleus (CCN) concentration and first indirect aerosol effect, Atmos. Chem. Phys., 8, 6325–6339, doi:10.5194/acp-8-6325-2008, 2008.

Wang, Y.Q., Zhang, X.Y. and Draxler, R., 2009. TrajStat: GIS-based software that uses various trajectory statistical analysis methods to identify potential sources from long-term air pollution measurement data. Environmental Modelling & Software, 24: 938-939

Ward, D. S., Eidhammer, T., Cotton,W. R., and Kreidenweis, S. M.: The role of the particle size distribution in assessing aerosol composition effects on simulated droplet activation, Atmos. Chem.Phys., 10, 5435–5447, doi:10.5194/acp-10-5435-2010, 2010.

Weber, R., P. H. McMurry, R. Mauldin, D. Tanner, F. Eisele, A. Clarke, and V. Kapustin,New particle formation in the remote troposphere: A comparison of observations at various sites, Geophysical Research Letters, 1999,26(3), 307-310.

Wex, H., Hennig, T., Salma, I., Ocskay, R., Kiselev, A., Henning, S.,Massling, A.,

678 Wiedensohler, A., and Stratmann, F.: Hygroscopic growth and measured and
679 modeled critical super-saturations of an atmospheric HULIS sample, Geophys. Res.
680 Lett., 34, L02818, doi:10.1029/2006GL028260, 2007.
681 Whitby, K., T.: The physical characteristics of sulfur aerosols. Atmos. Environ., 12,
682 135-159, 1967, Online publication date: 1-Jan-1978, 1978.
683 Wiedensohler A; Cheng YF; Nowak A; Wehner B; Achtelt P; Berghof M; Birmili W;
684 Wu ZJ; Hu M; Zhu T; Takegawa N; Kita K; Kondo Y; Lou SR; Hofeumahaus A;
685 Holland F; Wahner A; Gunthe SS; Rose D; Su H; Pöschl U (2009) Rapid aerosol
686 particle growth and increase of cloud condensation nucleus activity by secondary
687 aerosol formation and condensation: A case study for regional air pollution in
688 northeastern China, Journal of Geophysical Research: Atmospheres, 114**,** . doi:
689 10.1029/2008JD010884
690 Yue, D. L., Hu, M., Zhang, R. J., Wu, Z. J., Su, H., Wang, Z. B., Peng, J. F., He, L.Y.,
691 Huang, X. F., Gong, Y. G., and Wiedensohler, A.: Potential contribution of new
692 particle formation to cloud condensation nuclei in Beijing, Atmos. Environ., 45,
693 6070-6077, 2011.
694 Zhang, Q., Meng, J., Quan, J., Gao, Y., Zhao, D., Chen, P., and He, H.: Impact of
695 aerosol composition on cloud condensation nuclei activity, Atmos. Chem. Phys., 12,
696 3783-3790, doi:10.5194/acp-12-3783-2012, 2012.
697 Zhang, F., Z. Li, R. J. Li, L. Sun, C. Zhao, P. C. Wang, Y. L. Sun, Y. N. Li, X. G. Liu,
698 J. X. Li, P. R. Li, G. Ren, and T. Y. Fan., Aerosol hygroscopicity and cloud
699 condensation nuclei activity during the AC3Exp campaign: implications for cloud
700 condensation nuclei parameterization. Atmos. Chem. Phys., 14, 13423–13437,
701 2014
702
703

Figures

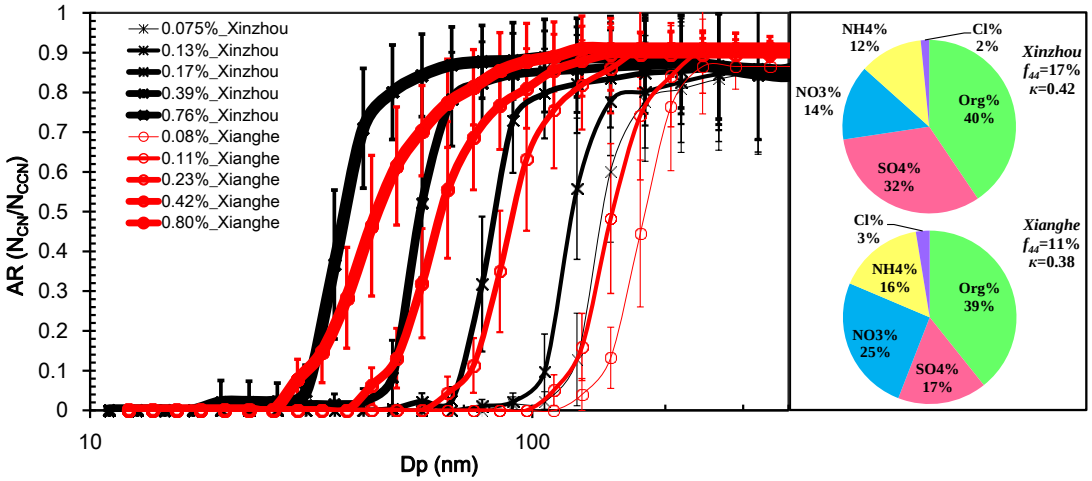

Fig. 1. Mean CCN efficiency spectra at the Xinzhou site (black lines with asterisks) measured from 22 July-26 August 2014 and at the Xianghe site (red lines with circles) site measured from 7-21 July 2013 for different supersaturation levels. Error bars representing one standard deviation are shown. Right panels show particle chemical composition in terms of mass concentration fractions at Xinzhou (top panel) and Xianghe (bottom panel) during their respective observation periods. The campaign average mass concentration of PM_1 is 31.6 μg m^{-3} and 72.4 μg m^{-3} at Xinzhou and Xianghe respectively. Note that the preset supersaturation levels were 0.07%, 0.1%, 0.2%, 0.4% and 0.8% at both sites, but effective supersaturation levels showed slightly different after calibration.

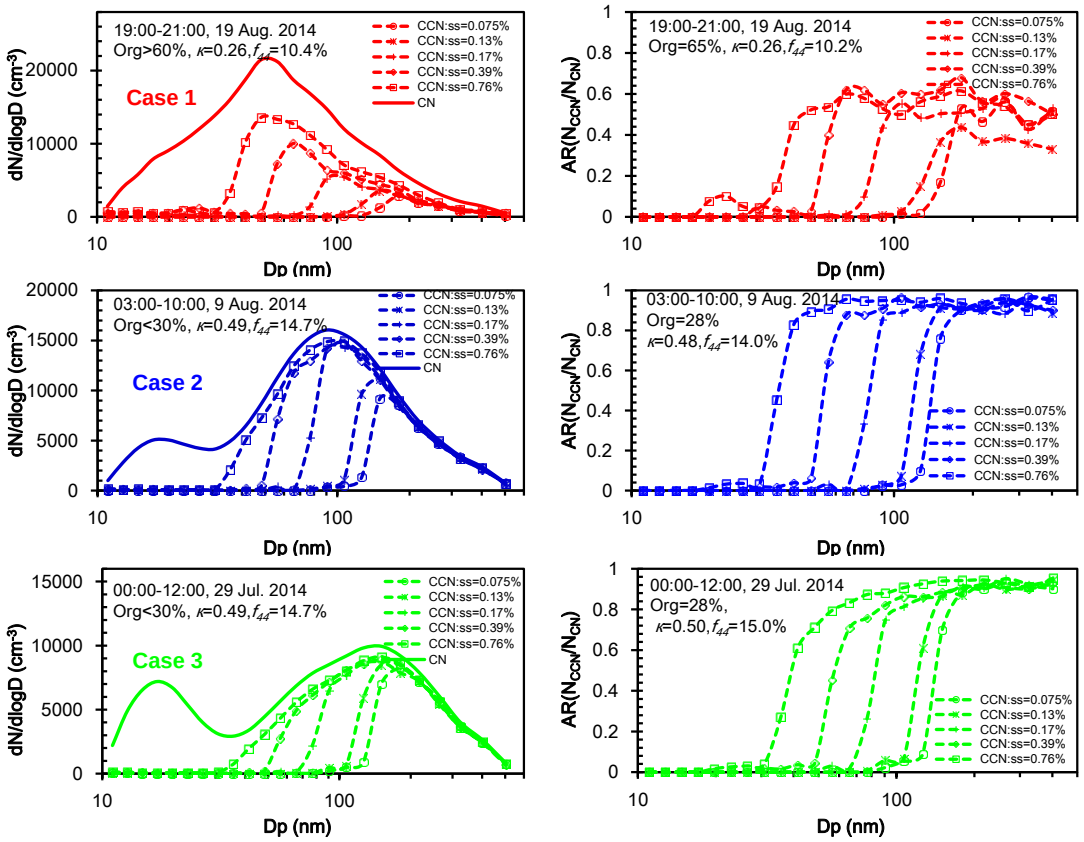

Fig. 2. Particle number size distribution (PSD) and CCN size distributions (left panels) and CCN efficiency spectra (right panels) at different supersaturation levels for Case 1 (upper panels, 19 August 2014, 19:00-21:00 LT), Case 2 (middle panels, 9 August 2014, 03:00-10:00 LT), and Case 3 (bottom panels, 29 July 2014, 00:00-12:00 LT). Total CN number concentrations are 16671 cm^{-3}, 12869 cm^{-3}, and 10134 cm^{-3} for Case 1, Case 2, and Case 3, respectively. Mass concentrations of PM_1 are 28.36 μg m^{-3}, 81.45 μg m^{-3}, and 78.73 μg m^{-3} for Case 1, Case 2 and Case 3, respectively.

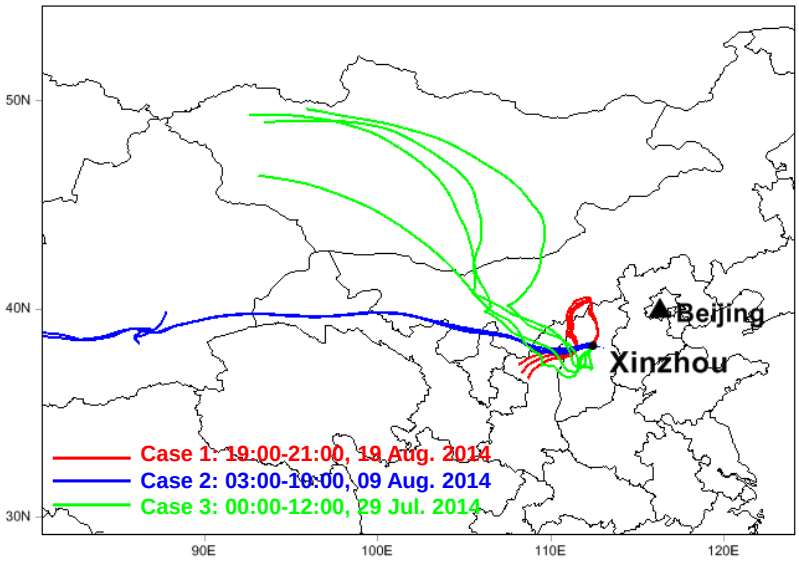

Fig. 3. Five-day back trajectories for Case 1 (in red), Case 2 (in blue), and Case 3 (in green) calculated using the Hybrid Single-Particle Lagrangian Integrated Trajectory model with National Centers for Environmental Prediction reanalysis data. The arrival height of the trajectories at the Xinzhou site was at the surface.

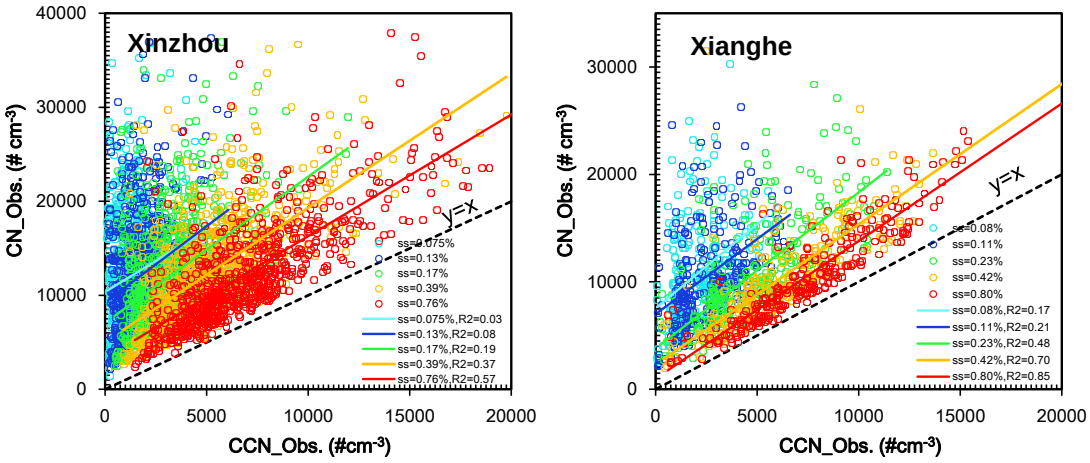

Fig. 4. Measured N_{CN} as a function of measured N_{CCN} for different supersaturation levels at the Xinzhou (left panel) and Xianghe (right panel) sites. The scatterplot between $CCN_{\_Obs}$ and CN_Obs. were fitted with a linear function (in colored lines) and R^2 refer to the correlations of them. .

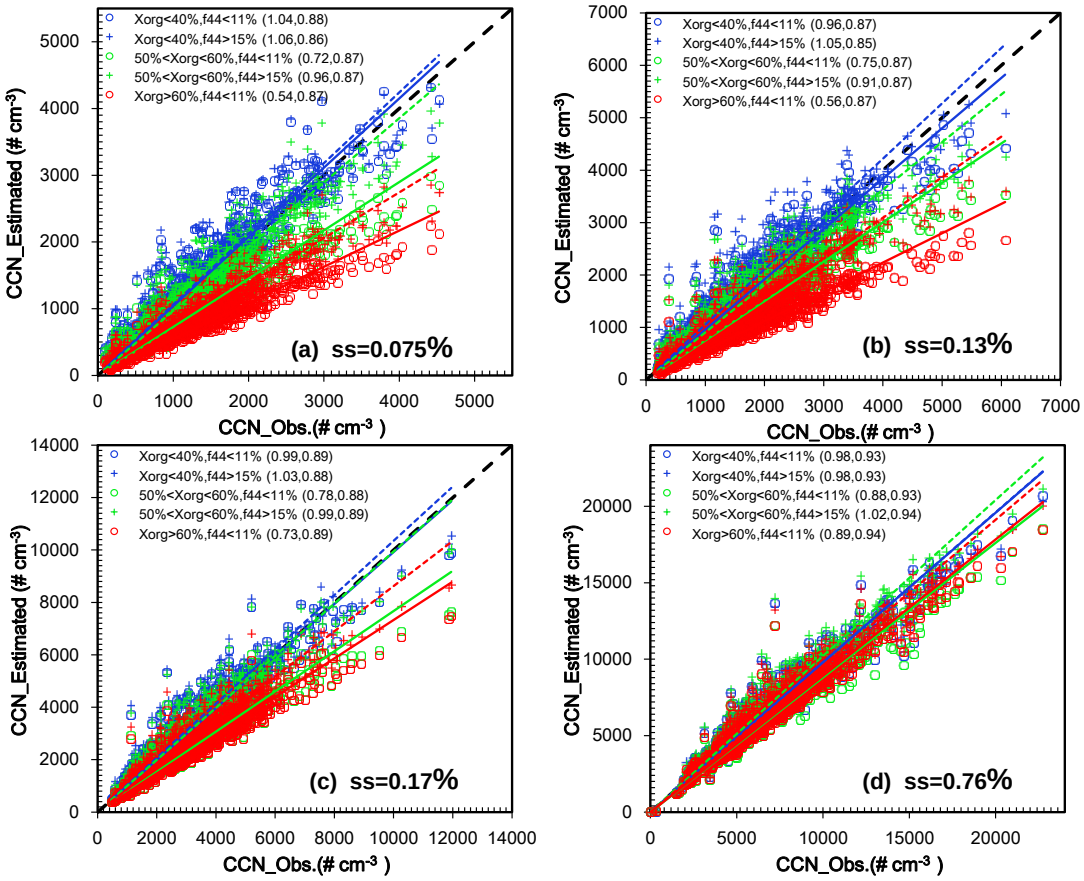

Fig. 5. The sensitivity of N_{CCN} to both organics volume fraction (x_{org}) and oxidation level (using f_{44}, the fraction of m/z 44 in aerosol organic material) of organics at supersaturation levels of (a) 0.075%, (b) 0.13%, (c) 0.17% and (d) 0.76% for cases when x_{org} = 35% (blue circles), 52% (green circles), and 66% (red circles). The size-resolved CCN data were sorted when the x_{org} >60 %, 50%<x_{org} <60 % and x_{org} <40 % respectively to do the sensitivity examination. Linear best-fit lines through each group of points are shown. Slopes and R^2 values are given in parentheses.

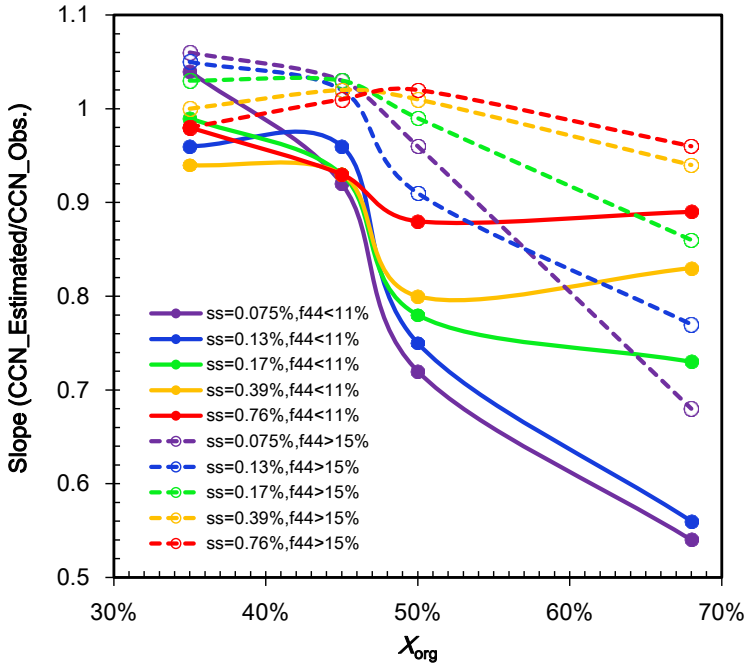

Fig. 6. Slopes of the linear fit of estimated and observed N_{CCN} dependence on volume fraction of organics (x_{org}) at f_{44}<11% and f_{44}>15% for different supersaturation levels. Mean values of the hygroscopic parameter κ_{chem} at f_{44}<11% when x_{org} >60 %, 50%<x_{org} <60 %, 40%<x_{org} <50 % and x_{org} <40 % are 0.27, 0.34, 0.40 and 0.46, respectively; while at f_{44}>15% the value increased to 0.36, 0.42, 0.46 and 0.50 respectively.

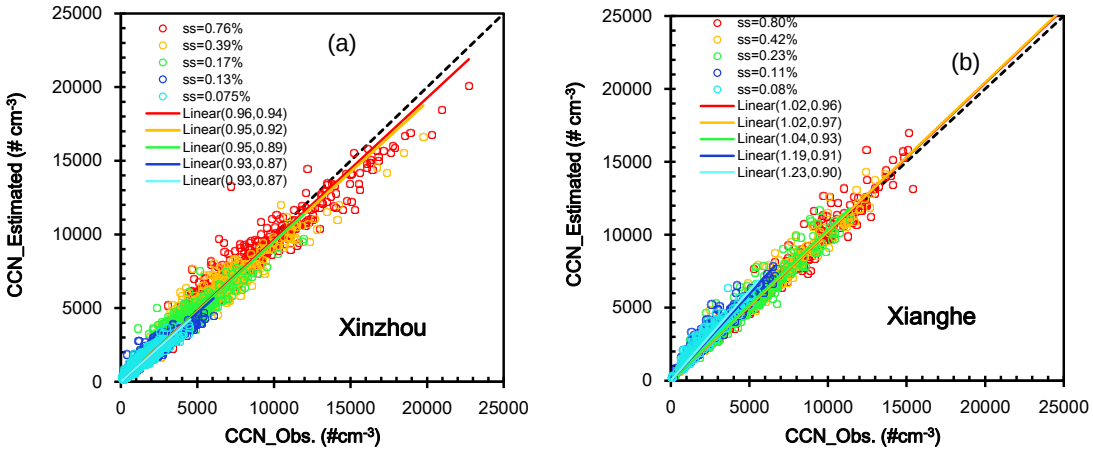

Fig. 7. Estimated N_{CCN} as a function of observed N_{CCN} for different supersaturation levels at (a) Xinzhou and (b) Xianghe. Note that the campaign mean CCN efficiency spectra at Xinzhou are used for estimating N_{CCN} at Xianghe. Linear best-fit lines through each group of points are shown. Slopes and R^2 values are given in parentheses.